Magnetic impurities in conducting oxides. I. $(Sr_{1-x}La_x)(Ru_{1-x}Fe_x)O_3$ system

A. Mamchik and I-Wei Chen*
Department of Materials Science and Engineering, University of Pennsylvania, Philadelphia, Pennsylvania 19104-6272, USA
(Received 24 June 2003; revised manuscript received 12 April 2004; published 20 September 2004)

The perovskite solid solution between ferromagnetic $SrRuO_3$ and antiferromagnetic $LaFeO_3$ is studied and its structural, electronic, and magnetic properties are reported. With increasing $LaFeO_3$, the solid solution forms a spin glass and undergoes, by Anderson localization, a gradual metal-insulator transition. Meanwhile, the saturation magnetization initially increases with $LaFeO_3$ concentration, signaling the formation of large, switchable local moments around Fe^{3+}. In addition, a large negative magnetoresistance emerges as the saturation magnetization decreases in the spin glass state. The solid solution is analogous to a Mn-doped, ferromagnetic Pd alloy that contains induced local moments around Mn impurities, which themselves interact antiferromagnetically. However, in $(Sr_{1-x}La_x)(Ru_{1-x}Fe_x)O_3$ the spin polarization of mobile electronic carriers persists even in Anderson localization and is the origin of the observed magnetoresistance. Similar magnetic and magnetoresistive behavior is expected in other 3*d* cation-containing ruthenates and possibly other conducting oxides.

DOI: 10.1103/PhysRevB.70.104409 PACS number(s): 75.30.Hx, 73.43.Qt, 75.50.Lk, 74.70.Pq

I. INTRODUCTION

Although there has been extensive research of magnetic impurities in metals over the last half century, similar studies in conducting oxides are few until recently. This is because oxide magnets are technologically important due to their electrical insulating attributes. Naturally, attention has been mostly directed toward reducing conductivity in magnetic oxides. In recent years, however, the research on colossal magnetoresistance has revealed an extremely rich variety of magnetic and conducting properties in complex oxides exhibiting an intricate coupling between mixed valency, Jahn-Teller distortion, and electron correlation, which leads to interrelated structural, magnetic, and metal-insulator transitions.[1] Up to the present time, though, such work is mostly limited to Mn-containing perovskites and related 3*d* transition metal oxides.

Compared to 3*d* transition metal oxides, metallic conductivity is rather more common among 4*d* and 5*d* transition metal oxides, although except ruthenates they rarely exhibit magnetism by themselves. For disordered, pseudocubic ABO_3 perovskites, the studies of Battle *et al.* on mixed $3d/4d/5d$ transition metal B sites (Fe/Nb, Fe/Ru, Fe/Ta, Fe/Ir, Co/Ru, Ni/Ru, Ni/Rh, Cu/Ru) found many spin glasses but thus far no evidence of a magnetic effect on electrical conduction.[2] In contrast, many B-site ordered perovskites of 3*d* and $4d/5d$ transition metals do possess both conductivity and long-range magnetic order.[3] Indeed, several such ordered perovskites, most prominently $Sr(Fe_{1/2}Mo_{1/2})O_3$, have been recently reported to have large magnetoresistance (MR) at relatively high temperatures.[4] Since the large MR observed is limited to polycrystals and not seen in single crystals or epitaxial thin films,[5] it is attributed to a grain boundary tunneling mechanism, similar to the one operating between granular ferromagnetic particles[6] but different from that in manganates. Nevertheless, these results provide evidence of a strong coupling between the 3*d* magnetic cations and the $4d/5d$ conducting electrons. A strong effect of 3*d* cations on the magnetic property of $CaRuO_3$ is also known.[7] For example, a small addition of Ti, Fe, Mn, and Ni changes $CaRuO_3$ from a paramagnetic to a ferromagnetic ground state, presumably because of a strong coupling between the 3*d* magnetic B-site cations and the 4*d* conducting electrons.

It is intuitively obvious that the strongest effect of magnetic cation substitution on conduction electrons should be felt in systems of the highest magnetic susceptibility. The theoretical basis of this argument was already provided in the classical studies of giant localized moments, e.g., induced by Fe and Mn impurities, in Pd which is endowed with a large susceptibility because of a very high electron density of states at the Fermi level $N(E_F)$. Among conducting oxides, $SrRuO_3$ and related compounds do have a high $N(E_F)$, so much so that they are either Stoner ferromagnets or on the verge of becoming one.[8] Indeed, we have made the first observations that several Fe-containing mixed ruthenates ($SrRuO_3$, $CaRuO_3$ and Sr_2RuO_4, forming substitutional solid solutions with $LaFeO_3$) exhibit surprisingly large MR at low temperatures, supporting a strong substitutional effect of magnetic cations on conduction electrons.[9] In agreement with the finding of Battle *et al.*, spin glass forms in these solid solutions. Yet a large MR occurs in the spin glass state, which is itself unusual since most other large-MR oxides possess long-range magnetic order instead.[1,4] This MR is not a grain-boundary phenomenon, since the MR measured in epitaxial thin films was identical to that obtained in the bulk ceramics. Moreover, these ruthenates lack such features as mixed valency, Jahn-Teller distortion, and structural/magnetic/metal-insulator transitions that are common in manganates. So their MR cannot operate by the same mechanisms either (field-assisted metal /insulator transition.) The present study on $Sr_{1-x}La_xRu_{1-x}Fe_xO_3$ covering the composition range up to $x=0.4$ is undertaken to further understand the origin of the MR mechanism and, more generally, the effect of 3*d* magnetic cation substitution on conducting oxides. Polycrystalline samples were used which, according to

TABLE I. Structure parameters for $Sr_{0.7}La_{0.3}Ru_{0.7}Fe_{0.3}O_3$ at room temperature. Space group: *Pnma* (No. 62). $a=5.5823(5)$ Å, $b=7.8489(2)$ Å, $c=5.5440(5)$ Å, $V=242.914(6)$ Å^3.

Atom	Site	x	y	z	U_{iso}(Å^2)	n
Sr	4*e*	0.5027(5)	1/4	0.99449(31)	0.0077(2)	0.7
La	4*e*	0.5027(5)	1/4	0.99449(31)	0.0064(2)	0.3
Ru	4*a*	0	0	0	0.0049(4)	0.7
Fe	4*a*	0	0	0	0.0037(6)	0.3
O1	4*e*	0.5430(14)	1/4	0.4957(68)	0.0151(8)	1
O2	8*f*	0.2723(16)	0.0199(11)	0.2316(20)	0.0151(8)	1

our previous work, should exhibit the intrinsic magnetic and MR behavior.

II. EXPERIMENTAL PROCEDURES

A. Materials

Ceramic samples of composition $Sr_{1-x}La_xRu_{1-x}Fe_xO_3$ ($0 \leqslant x \leqslant 0.4$) were prepared by the solution polymerization technique described elsewhere.[9,10] The method involved the thermal decomposition of a polymeric gel made from mixing RuO_2, nitrates of Sr, La, and Fe, and poly(ethylenglycol). After thermal decomposition, powders were pressed into pellets and sintered at temperatures between 1200 and 1400 °C while packed in an excess amount of sacrificial powder of $SrRuO_3$. The phase purity of the samples as well as their lattice parameters were studied by x-ray powder diffraction (XRD) using Cu $K\alpha$ radiation, with Si powder added as an internal standard. Crystal structure refinement was conducted for the powder sample with $x=0.3$ at the X-7A beam line (wavelength=0.5998 Å) at the National Synchrotron Light Source (NSLS) at Brookhaven National Laboratory. Only room temperature XRD data are reported here since no structural transition was found during cooling scans. The valence state of Ru of all the samples was determined by x-ray absorption near edge structure (XANES) on the Ru L_{III} edge in the fluorescence mode at the X19B beam line at NSLS. [Energy range=2820–2850 eV, selected by a Si(111), monochromator.] Magnetization data were collected in a physical property measurement system (PPMS) (Quantum Design) using rectangular bars with an aspect ratio of at least 2:1. The long axis was always along the direction of applied magnetic field since no magnetic anisotropy is expected for sintered polycrystals. For resistivity measurements pellets were cut into bars of approximate dimensions 8 mm $\times$1 mm$\times$1 mm, and the measurements were performed in a four-point-probe configuration in PPMS. The field direction was always perpendicular to the long axis of the bar since our previous work indicated little crystallographic MR anisotropy in the epitaxial thin film samples.[9] The MR was computed with reference to the zero-field resistance after the first complete field cycle to remove the effect of anisotropy due to the shape of the sample and possible irreversible changes.

III. RESULTS

A. X-ray diffraction

The crystal structure refinement for the $x=0.3$ sample was performed using the Rietveld method in the space group *Pnma* (No. 62) with the $SrRuO_3$ structure as the starting model.[11] A random placement of Sr and La on the Sr site, and Ru and Fe on the Ru site, at the nominal fraction of (0.7:0.3), was assumed. Atomic positions and isotropic thermal factors of ions were refined using the GSAS software package[12] with the peak shape function No. 3. The structure parameter data are presented in Table I, and the fitted XRD data are shown in Fig. 1. The refinement converged with values $R_p=2.26\%$ and $wR_p=2.72\%$ ($\chi^2=5.71$). The refined structure ($x=0.3$) is orthorhombic and slightly differs from that of $SrRuO_3$. Specifically, the unit cell volume increases from 242.26 Å^3 in $SrRuO_3$ to 242.91 Å^3, which is almost the same as that of $LaFeO_3$(242.88 Å^3). Correspondingly, the average B-O-B bond angle increases from 163° in $SrRuO_3$ to 165.4°, despite the smaller value of $LaFeO_3$ (157°).[13] Thus, Vegard's rule is not obeyed even though we did verify a complete range of solid solution between the two end members and detected no evidence for cation ordering on either A or B site. The XRD patterns of all the other samples also showed only a single orthorhombic phase. Fitted room temperature lattice parameters as well as volume of the unit cell are listed in Table II.

B. XANES

Our compositional design called for Fe^{3+} substitution of Ru^{4+} to be charge compensated by La^{3+} substitution of Sr^{2+}. This scheme was confirmed by ascertaining the Ru^{4+} state in our samples using Ru L_{III}-edge XANES spectra, shown in Fig. 2(b). They are compared with the spectra in Fig. 2(a)

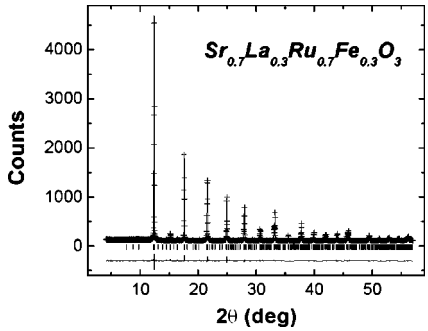

FIG. 1. Observed (cross) and calculated (solid line) x-ray diffraction profile from the Rietveld refinement of $Sr_{0.7}La_{0.3}Ru_{0.7}Fe_{0.3}O_3$. Tick marks indicate the positions of allowed Bragg reflections. The difference plot is shown at the bottom.

TABLE II. Summary of structure and magnetic data, as well as temperature for metal/insulator transition, in $Sr_{1-x}La_xRu_{1-x}Fe_xO_3$. Standard deviation of temperature (T) is estimated to be ±1 K, taking into account instrumentation precision (0.1 K), cooling /heating rate (2°/min), and sampling interval (1–3 K) for data which were then smoothed by interpolation. μ_{sat} is the average moment, in Bohr magneton, of each B-site cation, calculated from M(9 T) at 10 K using the conversion factor of 5584.8 emu/mol=1 μ_B.

x	0.0	0.1	0.2	0.23	0.25	0.27	0.3	0.4
a(Å)	5.5738(4)	5.5745(5)	5.5782(7)	5.5791(6)	5.5790(5)	5.5797(4)	5.5805(5)	5.5806(3)
b(Å)	7.8524(5)	7.8549(7)	7.8553(7)	7.8529(7)	7.8558(6)	7.8538(4)	7.8521(8)	7.86021(4)
c(Å)	5.5353(6)	5.5364(7)	5.5398(9)	5.5414(9)	5.5409(8)	5.5425(5)	5.5436(7)	5.54585(4)
V(Å^3)	242.265(1)	242.423(2)	242.745(2)	242.781(2)	242.842(2)	242.883(1)	242.926(2)	243.278(1)
T_C(K)	161	109	60.4	49.6	40.3	35		
T_f(K)			~5	19	30	35	39.5	47.6
T(K)		61	312	222	267	288	274	
θ_{CW}(K)	162.7(5)	128.8(4)	90.0(2)	83.8(4)	83.4(1)	74.4(3)	50.5(4)	−0.7(5)
$\mu_{eff}(\mu_B/\text{mol})$	2.608(3)	2.870(5)	3.009(2)	2.987(2)	2.925(1)	2.96(2)	3.089(3)	2.95(1)
$\mu_{sat}(\mu_B/\text{mol})$	1.3804(1)	1.6775(2)	1.3110(1)	1.1970(1)	1.0489(2)	0.9676(2)	0.5434(1)	0.2835(1)

(recorded in the same experiment) of the following model compounds: RuO_2, $CaRuO_3$, and $SrRuO_3$, all containing Ru^{4+}; and $SrY_{1/2}Ru_{1/2}O_3$, an ordered double perovskite containing Ru^{5+}. In general, the Ru L_{III}-edge XANES has two peaks which can be assigned to $2p \rightarrow t_{2g}$ and $2p \rightarrow e_g$ transition, respectively.[14] The two transitions in Ru^{5+} occur at higher energies than in Ru^{4+} because the 4d electrons of Ru^{5+} have lower energy levels, also the energy separation between the two transitions is larger in Ru^{5+} because of a stronger ligand field. These features of Ru^{5+} are clearly absent in all the $Sr_{1-x}La_xRu_{1-x}Fe_xO_3$ samples.

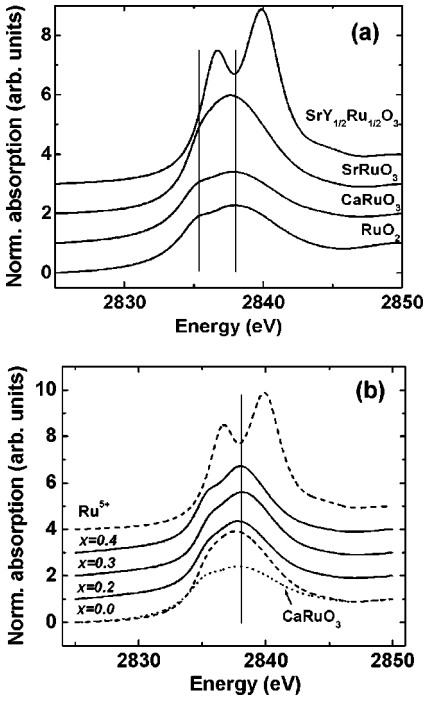

FIG. 2. Room temperature XANES spectra of ruthenate compounds: (a) spectra of model compounds: RuO_2, $CaRuO_3$, $SrRuO_3$, and $SrY_{1/2}Ru_{1/2}O_3$; (b) spectra of $Sr_{1-x}La_xRu_{1-x}Fe_xO_3$ samples with different composition x. Lines indicate positions of two transitions in the Ru^{4+} state.

C. Magnetic properties

The temperature dependence of molar dc magnetization is shown in Fig. 3 using data collected during cooling to 5 K in the magnetic field specified. The low field data of Fig. 3(a) verified that $SrRuO_3$ has a ferromagnetic transition (Curie temperature, T_C, at 162.26 K),[15] and that ferromagnetism weakens in the solid solution. The data at larger fields, shown in Fig. 3(b) for 1 T and in Fig. 3(c) for 9 T, show an unusual crossover of the $x=0.1$ and $x=0$ curves at low temperatures. This is confirmed in Fig. 4 which displays the field dependence of magnetization, $M(H)$, at 10 K, indicating a crossover field of about 1 T for the two compositions. Since the nearest neighbor (B site) Fe-Fe interaction is strongly antiferromagnetic (Neel temperature of $LaFeO_3$=740 K),[16] the extra magnetization in the $x=0.1$ sample at large fields cannot be due to Fe-Fe clusters, even if they exist. Therefore, it must come from the alignment of the local moment of Fe^{3+} under a high field. The "saturation" magnetization, M_{sat}, taken from M at 9 T at 10 K is plotted as a function of x in the inset of Fig. 4. A peak at $x=0.1$ and a rapid decrease at $x=0.3$ are evident.

Figure 5 displays the temperature dependence of the real part of ac susceptibility χ'_{ac} for all the compositions. With increasing x, the peak of χ'_{ac} occurs at lower temperature, which is similar to the behavior observed in Fig. 3. Note that the curves for $x=0.3$ and 0.4 are shown at ten times the actual values since the magnitude of χ'_{ac} has drastically decreased from $x=0.27$ to 0.3. Moreover, the shape of the χ'_{ac} peaks at $x=0.3$ and 0.4 is cusp-like, which is different from that at lower x. Such a cusp shape has been associated with spin glass in the literature,[2,17] which is reasonable given the competition between Ru-Ru (ferromagnetic) and Fe-Fe (antiferromagnetic) interactions, as well as the partitioning effect of Fe on the Ru-Ru network.

Other signatures of spin glass were also observed for these compositions. Figure 6 depicts the dc susceptibility curves of the $x=0.3$ sample obtained under the (0.01 T) field-cooled (FC) and zero-field-cooled (ZFC) conditions. A hysteresis is evident below the cusp temperature, which can

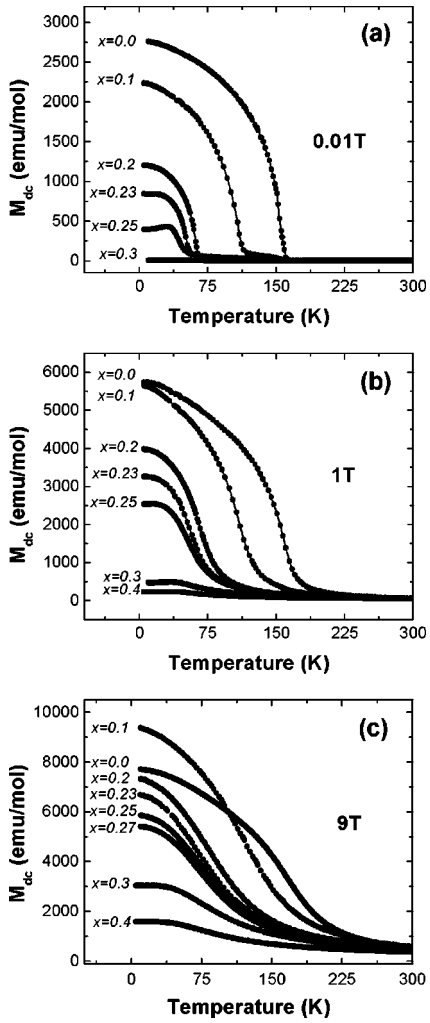

FIG. 3. Molar dc magnetization as a function of temperature for $Sr_{1-x}La_xRu_{1-x}Fe_xO_3$ samples with different composition x: cooling in (a) 0.01, (b) 1, and (c) 9 T.

be associated with the freezing temperature, T_f. Hysteresis is also manifest in Fig. 6 in the frequency dependence of the peak ac susceptibility, whose position shifts toward higher temperature at higher frequency indicating that freezing is frequency dependent. These observations strongly suggest

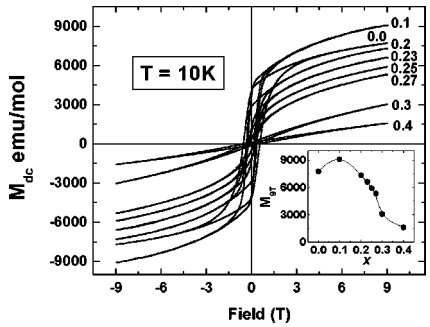

FIG. 4. Field dependence of dc magnetization at 10 K for $Sr_{1-x}La_xRu_{1-x}Fe_xO_3$ samples with different composition x. These curves were obtained using samples cooled to 10 K without a filed. Inset: magnetization at 9 T as a function of composition.

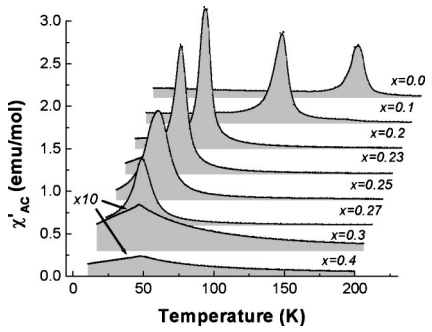

FIG. 5. Temperature dependence of real part of ac susceptibility of $Sr_{1-x}La_xRu_{1-x}Fe_xO_3$ samples with different composition x.

that the $x=0.3$ sample is a spin glass. The same holds for the $x=0.4$ sample.

For a normal ferromagnet the peak height of the ac susceptibility increases with decreasing T_C. Such a trend was observed for $0<x<0.2$. Beyond $x=0.2$, however, we find the peak height in Fig. 5 decreases with x, indicating a change in the magnetic behavior. This change was further investigated under different cooling and heating conditions. Figure 7(a) shows the magnetization curves obtained in the sequence of (i) strong field (1 T) cooled (SFC), (ii) zero-field-heated (ZFH), and (iii) weak field (0.01 T) cooled (WFC), for the $x=0.25$ sample. [The data of steps (i) and (iii) are from Fig. 3.] Also shown for reference are the data of χ'_{ac} during ZFH. It is clear that the SFC and WFC data are very different. This is already evident in Fig. 3 where the saturation magnetization at low temperature varies by a factor of 5 between SFC (1 T) and WFC (0.01 T) for $x=0.25$, compared to a factor of 2 for $x=0$. There is also a large difference in the magnetization between the SFC and ZFH cycle, which indicates that the large magnetization poled by the strong field cannot be retained at zero field in the ZFH cycle. From the ZFH curve, we further see that the sample loses most of its remnant magnetization at a temperature well below T_C, taken to be the peak temperature for χ'_{ac}. This is unlike the WFC case in which the largest magnetization change occurs over a temperature range around T_C. In comparison, in ferromagnetic $SrRuO_3$, there is an abrupt change in magnetization occurring at T_C in all the curves (SFC, WFC, and ZFH) shown in Fig. 7(b).

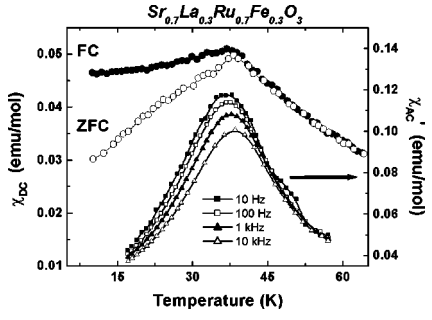

FIG. 6. Magnetic susceptibility of $Sr_{0.7}La_{0.3}Ru_{0.7}Fe_{0.3}O_3$ sample as a function of temperature showing spin-glass-like behavior, including deviation in the FC (0.01 T) and ZFC dc magnetic susceptibility below T_f and frequency dependence of ac susceptibility below T_f.

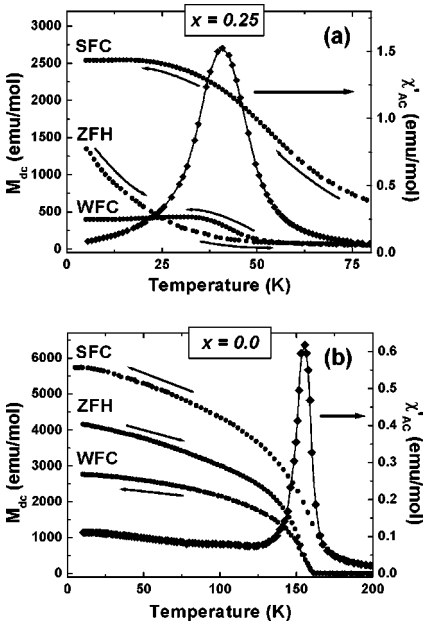

FIG. 7. Molar dc magnetization recorded following a SFC(1 T)/ZFH/WFC(0.01 T) measuring sequence. Real part of ac susceptibility during ZFH is also shown. (a) $Sr_{0.75}La_{0.25}Ru_{0.75}Fe_{0.25}O_3$ and (b) $SrRuO_3$.

Similar ferromagnetic behavior as $x=0$ was also seen in $x=0.1$ and 0.2 compositions, whereas similar behavior as $x=0.25$ was found in $x=0.23$ and 0.27 compositions. Thus, a clear distinction can be made between the ferromagnetic behavior of the samples with x up to 0.2, and those with $x=0.23, 0.25$, and 0.27. The behavior of the latter group is typical for cluster glasses, according to the literature.[17] In such materials, ferromagnetic interactions within each cluster are responsible for the WFC magnetization and the large ac susceptibility response at the apparent T_C (taken to be the peak-χ'_{ac} temperature, which is proportional to the strength of ferromagnetic interactions within each cluster.) Meanwhile, coupling between clusters, which is too weak to sustain a large remnant magnetization at zero field [the ZFH curve in Fig. 7(a)], is responsible for the SFC magnetization when the magnetic alignment between clusters is aided by an external field.

The earlier observations allow us to construct a tentative phase diagram for $Sr_{1-x}La_xRu_{1-x}Fe_xO_3$ in Fig. 8, showing the approximate phase boundaries of ferromagnetic (FM), cluster glass (CG), and spin glass (SG) state as the material is cooled from the paramagnetic (PM) state. For x from 0.2 to 0.25, we also found evidence for a reentrant transition from cluster glass to spin glass at a lower T_f. This CG/SG transition is manifested in several ways, for example, by a low temperature peak in $\chi''_{ac}(T)$, shown in Fig. 9(a). Even as T_C for the PM/CG transition and T_f for the CG/SG transition draw nearer and the latter transition is smeared by the former, the evidence for the CG/SG transition can still be seen in a shoulder in either $\chi'_{ac}(T)$ [Fig. 9(b)] or $\chi''_{ac}(T)$ (not shown.) Meanwhile, the T_f for the CG/SG transition is also responsible for a shoulder or a weak maximum in dc magnetization, as for $M(T)$ in ZFH [Fig. 9(b)] or in WFC (not

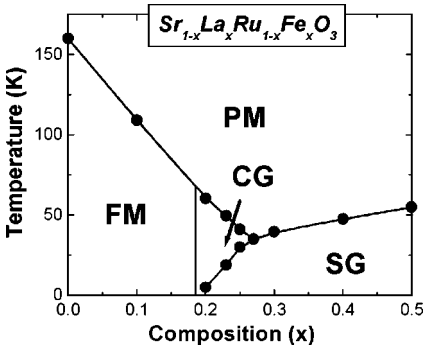

FIG. 8. Tentative magnetic phase diagram of $Sr_{1-x}La_xRu_{1-x}Fe_xO_3$ determined using ac/dc magnetization data. FM=ferromagnetic, PM=paramagnetic, CG=cluster glass, SG= spin glass.

shown.) These features were found for samples from $x=0.2$ to 0.25 but not for $x=0.27$ and higher. The phase boundary for the reentrant transition in Fig. 8 was drawn accordingly.

Magnetic behavior at $T>T_C$ was analyzed and it followed the Curie-Weiss law. The parameters, θ_{CW} and μ_{eff}, extracted from the fits of the FC(1 T) magnetization data are listed in Table II. The Curie-Weiss temperature continuously decreases with x, consistent with the weak-field magnetization data earlier. The effective magnetic moment, on the other hand, shows only a small increase. However, it is larger than the "saturation moment" μ_{sat} calculated from $M(9\ T)$, by a factor of 1.9 at $x=0$ and 5.7 at $x=0.3$. **(**Theoretically, this ratio, $[(S+1)/S]^{1/2}$, should be 1.4 for $S=1$.**)** The Rhodes-Wohlfarth ratio deduced from μ_{eff} and μ_{sat} in the ferromagnetic compositions varies from 1.3 for $x=0$ to 1.7 for $x=0.2$, indicating a mixed nature of itinerancy and localization for the magnetic moments.[18]

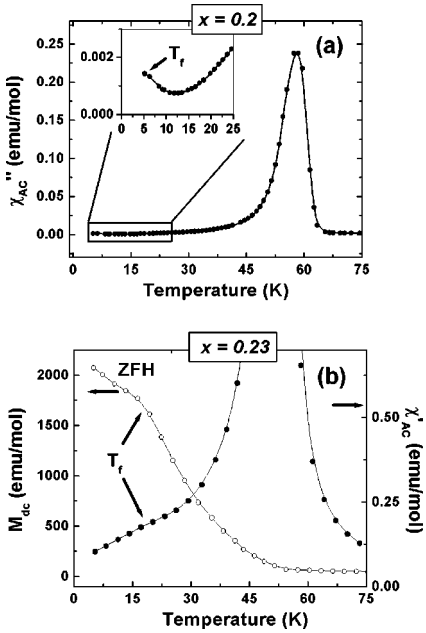

FIG. 9. Determination of T_f, marked by arrows, in cluster glass from a combination of ac/dc magnetization measurements. (a) $Sr_{0.8}La_{0.2}Ru_{0.8}Fe_{0.2}O_3$, and (b) $Sr_{0.77}La_{0.23}Ru_{0.77}Fe_{0.23}O_3$.

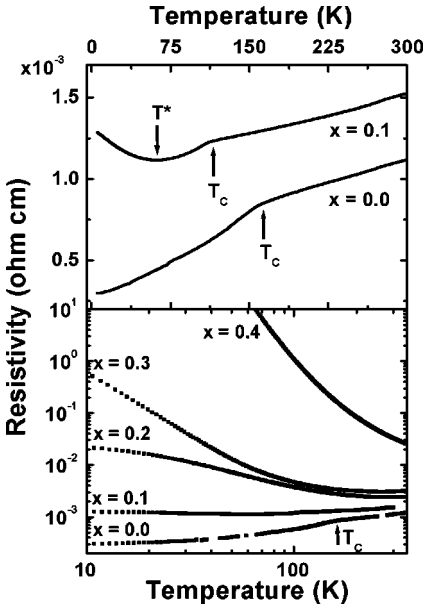

FIG. 10. Temperature dependence of resistivity for $Sr_{1-x}La_xRu_{1-x}Fe_xO_3$ samples with different composition x. The data of $x=0$ and 0.1 are plotted in different scale on the top to make obvious the kink at T_C and the resistivity minimum at T^*.

D. Electrical resistivity

The resistivity $\rho(T)$ of metallic $SrRuO_3$ displays a kink at T_C because of a change in the magnetic scattering of conducting electrons. On our data, shown in Fig. 10, this is marked by an arrow at 160 K. Substitution with $LaFeO_3$ eventually led to an apparent metal-semiconductor transition at the temperature T^*, empirically defined as the minimum resistivity temperature on the curve, with metallicity prevailing at $T>T^*$. (See the upper panel of Fig. 10 for an example in the $x=0.1$ sample.) In agreement with the magnetic data, T_C decreases with x, but T^* roughly increases with x. These features are absent in some curves. For example, no kink appears when the magnetic transition occurs on the semiconductor side, as in $x=0.2$ for which $T_C<T^*=220$ K. For $x=0.4$ no metallic behavior was observed up to at least 350 K. These data are also summarized in Table II.

The semiconducting data at low temperatures range appear to follow the variable range hopping model.[19] In Fig. 11 we plot $\log(\sigma)(\sigma=\rho^{-1})$ vs $T^{1/4}$. The linear dependence for the $x=0.3$ and 0.4 sample is in accord with the model prediction $\rho(T)=\rho_0\exp(T_0/T)^{1/4}$. The typical hopping length, predicted to be $r=a(T_0/T)^{1/4}$ with a being the effective Bohr radius of an electron localized around its trapped site, was calculated from these data. The average hopping range at 10 K and zero field were about 8 a for $x=0.3$ and 28 a for $x=0.4$, and slightly shorter at high field.

E. Magnetoresistance

Upon the application of a magnetic field the sample resistivity generally decreased, giving rise to a large negative MR in some compositions. An example is illustrated in the inset of Fig. 12 using the resistivity of the $x=0.3$ sample at zero field and 9 T, both collected during cooling. The negative MR, defined as $(\rho_0-\rho_H)/\rho_0$, is shown in Fig. 12 for several samples at 9 T. (Other compositions were omitted for clarity.) Unlike $SrRuO_3$, which has a small MR that peaks at T_C,[20] our samples showed monotonically increasing negative MR with decreasing temperature, except for the $x=0.1$ sample that is strongly ferromagnetic. We have determined the field dependence of MR for all the compositions at 10 and 30 K and found that the largest negative MR occurs at $x=0.3$. As illustrated in Fig. 13, the MR at 10 K has a symmetric field dependence that lacks the cusplike feature commonly associated with grain boundary tunneling MR.[4]

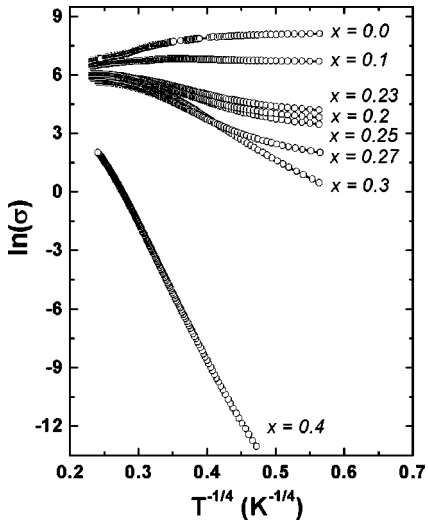

FIG. 11. Log of conductivity (σ) as a function of $T^{-1/4}$ for $Sr_{1-x}La_xRu_{1-x}Fe_xO_3$ samples with different composition x.

The magnetization dependence of MR proves most revealing. At a constant temperature, say 10 K, this can be inspected by crossplotting the $M(H)$ data of Fig. 4 and MR(H) data of Fig. 13. The result shown in Fig. 14 suggests a roughly linear relationship between MR and M^2. Indeed, for $x=0.27$ and above (in the spin-glass state) where there is no remnant magnetization at all, the plots are essentially linear. The average slope, $MR_{9\ T}/(M_{9\ T})^2$, shown in the inset of Fig. 14 for 10 and 30 K, rapidly increases with composition for $x>0.27$. This suggests that the ferromagnetic magnetiza-

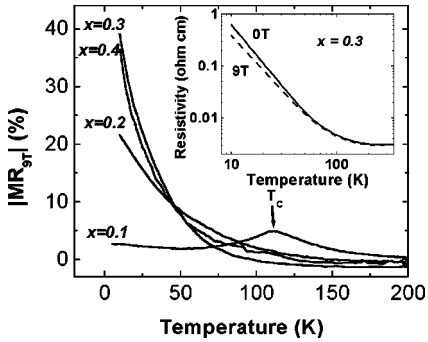

FIG. 12. Temperature dependence of 9 T MR for $Sr_{1-x}La_xRu_{1-x}Fe_xO_3$ samples with different composition x. Inset: temperature dependence of resistivity for the $x=0.3$ sample in zero field and 9 T.

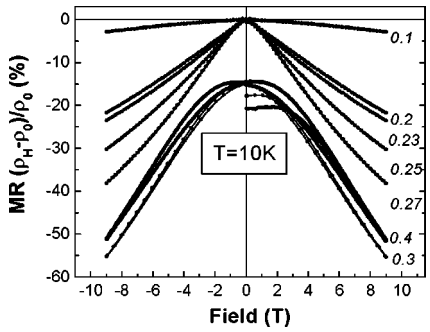

FIG. 13. Field dependence of MR at 10 K for $Sr_{1-x}La_xRu_{1-x}Fe_xO_3$ samples with different composition x. The data of $x=0.3$ and 0.4 have been shifted downward by 15% for clarity. The resistance was recorded during a field sweep from 0 to +9 to −9 T and back to 0 T. These sweeps found little hysteresis indicating very little shape anisotropy in ferromagnetic samples. However, in ZFC spin-glass samples below T_f some irreversible changes occurred during the first field sweep.

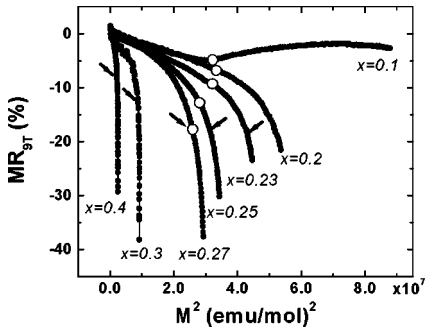

FIG. 15. MR vs dc M^2 at a constant field (9 T) for data collected at different temperatures, for $Sr_{1-x}La_xRu_{1-x}Fe_xO_3$ samples with different composition x. Temperature, which decreases with increasing M^2, is an implicit parameter for these curves. Where applicable, open circle indicates M^2 value at T_C, and arrow indicates M^2 value at T_f.

tion, present in the low x samples, is not responsible for the MR. The MR-M^2 relation can also be inspected by crossplotting $M(T)$ data of Fig. 3 and the MR(T) data of Fig. 12, with the field fixed at, say, 9 T. This is shown in Fig. 15 in which all the curves except one ($x=0.1$) exhibit a characteristic shape plunging toward an asymptotic M value, which corresponds to the saturation magnetization at 0 K. In this regime, while magnetization is nearly saturated, MR continues to rapidly increase with decreasing temperature. These curves also show no special feature at either T_f (indicated by arrow) or T_C (circle). The exception of $x=0.1$ is again due to its strongly ferromagnetic character, as evident from the peak MR that concides with $M(T_C)$ as indicated by the marker.

IV. DISCUSSION

A. Energy levels and magnetic interactions of *d* electrons

Ferromagnetism of $SrRuO_3$ has been attributed to itinerant d electrons and explained in terms of the Stoner criterion.[8] However, there is also clear evidence for local moments in this compound, judging from the Curie-Weiss behavior of magnetic susceptibility above the Curie temperature. This dual character of d electrons is commonly reconciled in the framework of spin-fluctuation theory of Moriya that simultaneously allows spin/charge itinerancy and localization in both the real and the k space.[18] For $SrRuO_3$ and the ferromagnetic solid solutions studied here (up to $x=0.2$), the Rhodes-Wohlfarth ratio is from 1.3 to 1.7, which is an intermediate value consistent with the earlier interpretation. The Stoner ferromagnetism in $SrRuO_3$ is attributed to the high $N(E_F)$ as a consequence of the narrow ($4d$) band width and the presence of a van Hove singularity.[8] So, A- or B-site substitution tends to weaken the ferromagnetism by shifting either $N(E_F)$ or the van Hove singularity,[20] lowering T_C and θ_{CW}.[7,21,22] Meanwhile, since $SrRuO_3$ is a "bad metal,"[23] the screening length is likely to be long and the Coulomb interactions, including electron correlation, are not fully screened over one B-O-B distance. In the subsitutional solid solutions, further electron localization in the Anderson sense also occurs because of the charge and size disorder at the substituted sites. The earlier picture suggests that we may consider pairwise cation-cation magnetic interactions, J_{RuRu}, J_{FeFe}, and J_{FeRu} to understand the magnetism in the solid solutions. Obviously, J_{RuRu} is ferromagnetic and positive but its magnitude decreases with substitution. Meanwhile, J_{FeFe} is antiferromagnetic and strongly negative in view of the Fe-O-Fe superexchange interaction for the high-spin Fe^{3+} ($3d^5$) cations.[16] The competing J_{RuRu} and J_{FeFe} interactions therefore lead to a spin glass state in the (B) site Ru-Fe solid solutions.[17] The more interesting question is whether J_{FeRu} is ferromagnetic or antiferromagnetic. In the following, we will argue that it is ferromagnetic and it lead to the formation of ferromagnetic Ru^{4+} clusters around Fe^{3+}, and, eventually, to a large negative MR.

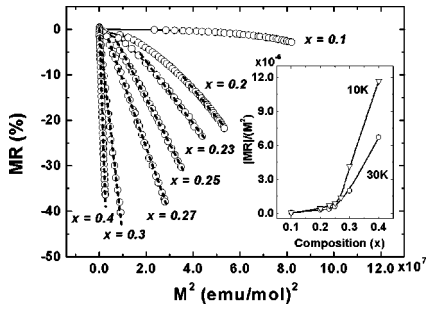

FIG. 14. MR vs dc M^2 at a constant temperature (10 K) for data collected at different fields, for $Sr_{1-x}La_xRu_{1-x}Fe_xO_3$ samples with different composition x. Field, which increases with increasing M^2, is an implicit parameter for these curves. Dashed lines on the curves are linear fit to data. Inset: compositional dependence of ratio of $MR_{9\ T}/M^2_{9\ T}$ at 10 and 30 K.

The ferromagnetic J_{FeRu} arises because of electron resonance between Fe^{3+} and Ru^{4+}. This motivates the net spin of Ru^{4+} electrons (low-spin $S=1$) to align with that of Fe^{3+} (high-spin $S=5/2$), i.e., they adopt the Ru^{4+} $t_{2g}\uparrow^3 t_{2g}\downarrow^1$ and Fe^{3+} $t_{2g}\uparrow^3 e_g\uparrow^2 t_{2g}\downarrow^0$ configurations, with the resonance electron being the $t_{2g}\downarrow$ type. A direct verification of the ferromagnetic coupling between Ru^{4+} and Fe^{3+} would have been pos-

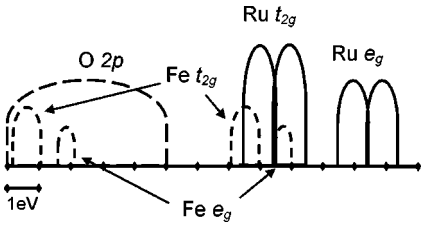

FIG. 16. Schematic energy diagram for the electron levels in $Sr_{1-x}La_xRu_{1-x}Fe_xO_3$. In constructing the diagram, we used data in Ref. 24 to define the Zaanen-Sawatzky-Allen energies $(\Delta, U, 10Dq)$.[40] In units of electron-volts, they are $(3, 1.7, 3)$ for Ru^{4+} and $(2.6, 7, 1.3)$ for Fe^{3+}. We also let band width W be 1 eV for all the t_{2g} and e_g bands.

sible if the $x=0.5$ compound were B-site ordered. However, due to the relatively small mismatch between the size and charge of Ru^{4+} and Fe^{3+}, this compound is disordered and forms a spin glass instead. On the other hand, the analogous $Sr(Mo_{1/2}Fe_{1/2})O_3$ compound with an electronic structure of Mo^{5+} $t_{2g}\downarrow^1$ and Fe^{3+} $t_{2g}\uparrow^3 e_g\uparrow^2 t_{2g}\downarrow^0$ is ordered.[4] Here, a similar resonance of $t_{2g}\downarrow$ elecron between Mo^{5+} and Fe^{3+} should compel the net spins of Fe^{3+} and Mo^{5+} to become antiparallel, which is the case since the compound is ferrimagnetic. Therefore, this resonance mechanism between 3*d* and 4*d* electron orbitals seems viable and, around each Fe^{3+}, it leads to a ferromagnetic shell of Ru^{4+} with its net spin aligned with that of Fe^{3+}.

To justify electron resonance, the energy levels of the $Ru^{4+}(t_{2g}\downarrow^1)$ band and the $Fe^{3+}(t_{2g}\downarrow^0)$ band need to be close. This is obviously the case of the $t_{2g\downarrow}$ electrons of Mo^{5+} and Fe^{3+}, since $Sr(Mo_{1/2}Fe_{1/2})O_3$ is metallic having nearly completely spin-polarized *d* electrons; i.e., it is "half-metallic."[4] The situation of $Sr_{1-x}La_xRu_{1-x}Fe_xO_3$ is less obvious because of the random placement of A- and B-site cations. To gain some insight, we will assume that the relative energy levels of the *d* electrons of the B-site cation, measured from the top of the oxygen 2*p* manifold, are invariant when the cation environment changes from the "pure" $(SrRuO_3/LaFeO_3)$ state to the solid solution $(Sr_{1-x}La_xRu_{1-x}Fe_xO_3)$ state. This assumption allows us to construct the schematic energy diagram in Fig. 16 for the *d* electrons of Ru^{4+} and Fe^{3+} in $Sr_{1-x}La_xRu_{1-x}Fe_xO_3$ using their respective energy levels in $SrRuO_3$ and $LaFeO_3$, which are known from first-principles calculations and spectroscopy.[24] It is then clear that the (empty) Fe $t_{2g\downarrow}$ levels are located close to the (partially occupied) Ru $t_{2g\downarrow}$ levels. Therefore, electron resonance is plausible in $Sr_{1-x}La_xRu_{1-x}Fe_xO_3$ and may give rise to a positive J_{FeRu}.[25]

This energy diagram is supported by the XANES spectra which probe the unoccupied part of the electronic density of states. The process is fast enough that only the local environment, RuO_6 octahedron, is most relevant. The XANES peaks in Fig. 2 assigned to O $2p\rightarrow$Ru t_{2g} and O $2p\rightarrow$Ru e_g transitions thus reflect the energies and the numbers of the empty Ru states.[14] Compare the spectra of (i) Ru^{4+}, as in $CaRuO_3$, (ii) Ru^{5+}, as in $SrY_{1/2}Ru_{1/2}O_3$ and (iii) Ru^{4+} in the presence of neighboring Fe^{3+}, as in $Sr_{1-x}La_xRu_{1-x}Fe_xO_3$, we find $10Dq$ (the energy difference between the two peaks) is about 3 eV for Ru^{4+}, which is consistent with our assumption in constructing Fig. 16 and the previous spectroscopic data.[24] Comparing (i) and (iii), we see that there is no shift in the transition energies, but the low energy transition is stronger in (iii) indicating more empty states in Ru t_{2g}, possibly because of an electron transfer to Fe^{3+}. This is consistent with our picture since the resonance we envisioned is a real transition and not a virtual transition. (Similar observations have been reported in $SrFe_{1/2}Mo_{1/2}O_3$, in which the Fe band is strongly hybridized with the Mo band. The electronic density shifts from Mo^{5+} to Fe^{3+} in this ordered compound, thus creating, in some experiments, evidence for the intermediate Fe valence states, between 2+ and 3+.[26]) Comparing (i) and (ii), we see that both transition energies and their separation $(10Dq)$ are higher in (ii), which is expected from the higher valence state of 5+. The weight of the low energy transition is also higher in (ii) reflecting one fewer electron in Ru t_{2g}. In short, the general consistency between the XANES spectra and Fig. 16 lends credence to our picture of energy levels, electron resonance, and ferromagnetic coupling between Ru^{4+} and Fe^{3+}.

B. Substitution-induced magnetic moment

To recast the discussion of Fe-Ru interaction in terms of delocalized electrons, we note that the Fe^{3+} $t_{2g}\uparrow^3 e_g\uparrow^2$ band is full and well separate from the conduction (Ru^{4+} t_{2g}) band, thus Fe^{3+} is a localized magnetic "impurity"[27] with empty $(t_{2g}\downarrow)$ states that happen to be near the Fermi surface of the (Ru t_{2g}) conduction electrons. As a result, it can form virtual bound states with conducting electrons. The situation is similar to that of 3*d* magnetic impurities in 4*d* metals, e.g., Fe dissolved in Pd, which induces giant magnetic moments, even ferromagnetism.[28,29] Magnetism in both cases involves only *d* electrons for which the theory of Wolff, Clogston, and co-workers is applicable.[30,31] Following this theory, we expect the scattering cross section of the conduction (Ru)*d* electrons by the (Fe^{3+}) magnetic impurity potential to experience a maximum near E_F, due to a resonance at the empty impurity (Fe^{3+} $t_{2g}\downarrow$) state. Since only the down-spin conduction electrons near the E_F can benefit from the resonance, the corresponding Wannier functions located at the nearby sites will also favor the down-spin type. Therefore, the nonparticipating filled band of Ru t_{2g} will be of the up-spin type at these locations, and will be largely responsible for the (net up) moment for Ru which is in alignment with the local (up) moment of Fe^{3+}. As further shown by Clogston *et al.*, the induced magnetic polarization of the surrounding conducting electrons in the host metal is proportional to $N(E_f)$, which is very high in Pd,[32] $SrRuO_3$, and $CaRuO_3$. This again justifies the positive J_{FeRu}.

For $CaRuO_3$, which is paramagnetic, we have already reported induced ferromagnetism due to $LaFeO_3$ substitution.[9] For ferromagnetic $SrRuO_3$, evidence for induced magnetic moments is manifest in the crossover of the magnetization curves in Figs. 3(c) and 4, giving the maximum in the saturation magnetization at $x=0.1$. Since the crossover field is proportional to the crossover temperature [1.5 T at 10 K in Fig. 4, 9 T at 100 K in Fig. 3(c)], the crossover is indicative

of the field-induced rotation of certain magnetic moments. On the other hand, the moment of $Fe^{3+}(S=5/2)$ itself is too small to rotate with a field of the earlier magnitude at these temperatures, in view of the large magnetic anisotropy energies typically associated with Fe^{3+} in oxides. Therefore, the rotation strongly implies a much larger effective moment which we believe is induced by the Fe^{3+} polarization of the neighboring electrons.

In paramagnetic Pd, the range of Fe-induced ferromagnetic alignment extends to more than 1 nm from the impurity, according to neutron scattering data and electronic structure calculations.[33] In $Sr_{1-x}La_xRu_{1-x}Fe_xO_3$ we can indirectly estimate the range by noting the maximum magnetization occurs at $x=0.1$. Comparing this composition with the probability of finding a nearest B-site neighbor $(1/6)$ and a next nearest neighbor $(1/12)$, we conclude that the polarization cloud probably does not extend beyond the nearest Fe-Ru pairs (0.4 nm). At higher Fe concentrations, the impingement of the polarization clouds overlaps, so the effective moment decreases. In addition, there is an increasing chance to form Fe-Fe nearest neighbors (on the B sublattice), which interact antiferromagnetically and cannot be aligned by the field, so the effective moment also decreases. The probability of finding Fe-Fe nearest neighbors at any B site is $6x^2$ in the case of random B-site substitution, or 6% at $x=0.1$ and 24% at $x=0.2$, increasing rapidly with x. Therefore, it is not surprising that the maximum magnetization is reached at a relatively small x given the strongly negative J_{FeFe}.

In this respect, a comparison with Pd(Mn,Fe) alloy is instructive. Like Fe, Mn also induces giant moments in Pd.[29] However, unlike Fe, short-range Mn-Mn interaction in Pd is antiferromagnetic whereas Fe-Fe interaction in Pd is ferromagnetic. Thus, as the amount of Mn in Pd increases, the effective moment induced by Mn eventually decreases.[34] For a Pd-0.35%Fe host alloy, which is ferromagnetic because of Fe doping, the addition of Mn actually causes the alloy to undergo a transition from ferromagnetic to spin glass, with a reentrant ferromagnetic-to-spin glass transition occurring at an intermediate composition.[35] Obviously, this behavior is similar to the phase diagram (Fig. 8) of $Sr_{1-x}La_xRu_{1-x}Fe_xO_3$. The amount of Mn required (about 6%) to render the Pd alloy a spin glass, however, is much lower than that of Fe^{3+} (about 27%) for the ruthenate. This can be accounted for by (i) the larger number (12) of nearest neighbors in (face-centered-cubic) Pd compared to that (6) of B sites in perovskite, and (ii) antiferromagnetic Mn-Mn interaction extends to the (6) next nearest neighbors in Pd but antiferromagnetic Fe^{3+}-Fe^{3+} interaction extends only to the nearest neighbors.

C. Magnetoresistance

The large negative MR observed in $Sr_{1-x}La_xRu_{1-x}Fe_xO_3$ cannot be associated with Lorentz force or ferromagnetic transition.[20] MR due to Lorentz force should be positive, which contradicts our observation. MR due to ferromagnetic transition should peak at T_C, which is not the case here except for $x=0$ and 0.1 when the MR is relatively small. Besides, $SrRuO_3$ and $CaRuO_3$ have comparable metallic resistivity but only $SrRuO_3$ is ferromagnetic. Previously, we have proposed that an atomic spin valve mechanism, involving a bridging Fe^{3+} electron state between two Ru^{4+} electron states, can explain how the Fe moment regulates the conduction of Ru electrons. This mechanism is further developed later in view of our current understanding of the polarization and localization behavior in $Sr_{1-x}La_xRu_{1-x}Fe_xO_3$.

In the regime where strong MR is seen, the resistivity is several orders of magnitude above that of $SrRuO_3$. Therefore, very few mobile carriers are available in these compositions. Yet their concentration or transport mechanism must be highly sensitive to the overall magnetization since MR linearly rises with M^2. Meanwhile, since Anderson localization occurs at Fe^{3+} and La^{3+} substitution sites, forming localized states outside the energy bands of $SrRuO_3$, only those carriers that occupy states at energies lying beyond the mobility edge are mobile. We now argue that these mobile carriers, whose concentration (i.e., conductivity) must rapidly decrease with x as the localized states proliferates, are highly spin polarized. This is because, as the electron states near Fe^{3+} are magnetically polarized, they are split into majority "bands" and minority bands just like in a ferromagnet. Therefore, since there are more occupied states in the majority bands than in the minority bands, there are also more mobile electrons in the majority band than in the minority band, given the same relative energy level of the mobility edge in these bands. As a result, the mobile carrier population in any "ferromagnetic" cluster, while very sparse, is always highly spin polarized just like in a metallic ferromagnet. Electron conductivity, therefore, depends on the correlation of the majority spin whose orientation varies from one Fe-centered ferromagnetic cluster to another. This correlation depends on the overall magnetization, hence, the MR.

We now consider the simplest model with only two orientations, up and down, for the spin. The probability of finding a cluster in the up state is $(1+m)/2$, where m is M/M_{sat}, and likewise for the down state is $(1-m)/2$. Next, the probability for spin alignment in two neighboring clusters, either both up or both down, is $[(1+m)^2+(1-m)^2]/4$. Therefore, the resistivity, which inversely scales with this probability, is proportional to $2/(1+m^2)$. This implies a negative MR of $m^2/(1+m^2)$. This prediction is consistent with our observation of the strong M^2 dependence. Importantly, since it predicts that the slope in Fig. 13 should inversely scale with M_{sat}^2, whereas M_{sat} rapidly decreases when $x>0.27$, it explains why a larger MR is obtained at a higher x when compared at the same magnetization.

The earlier simple prediction is only valid at small m and when the placement of magnetic substitutional cations is random. At higher m, conductivity percolation needs to be considered, which would lead to a more rapid decrease in resistivity. (Otherwise the maximum MR is 50% according to the earlier prediction.) This, however, will be countered by the antiferromagnetic coupling between Fe^{3+} cations, since around a $Fe\uparrow$-$Fe\downarrow$ pair the polarization cloud is poorly developed. On the other hand, if the magnetic substitutional cations are orderly placed between every two Ru, it is conceivable that the compound may experience a field-induced transition from a completely insulating, antiferromagnetic (or

ferrimagnetic) state to a conducting ferromagnetic state, giving a MR of 100%. Although most antiferromagnetic oxides probably are not switchable because of the very high switching field required, a relatively large MR (8%) has been recently reported in antiferromagnetic $SrY_{1/2}Ru_{1/2}O_3$ at 10 T at 17 K.[36]

V. CONCLUDING REMARKS

In this study, we have shown that the structure and valence states of $Sr_{1-x}La_xRu_{1-x}Fe_xO_3$ are quite normal, without any transition or mixed valence throughout the composition range studied. The magnetic phase diagram is also prototyptical for a binary substitutional solid solution of ferromagnetic and antiferromagnetic end members. The solid solution undergoes a gradual metal /insulator transition due to Anderson localization, which is again expected because one end member ($LaFeO_3$) is a Mott insulator. The main effects of magnetic Fe substitution are (a) the polarization of neighboring conducting electrons, giving rise to a large effective moment around Fe, which enables a relatively modest field to align these substitutional cations at relatively high temperatures, and (b) a robust negative MR in the insulating, spin-frustrated states when host ferromagnetism already fades away. The first effect can be explained by drawing an analogy with the case of Fe (and Mn) impurities in Pd, noting that the very high $N(E_F)$ of the host and the unoccupied electron states of the magnetic impurity at energies near E_F provide intense virtual bound states and induce a strong magnetic polarization of the conducting electrons. The second effect can be explained by noting that the population of mobile carriers is strongly spin polarized even under Anderson localization, provided the localization occurs around polarizing magnetic substitutional cations. In addition to the requirements of (i) energy alignment between the magnetic substitutional cation and the host conduction band, and (ii) a high $N(E_F)$ of the host, some (iii) electron localization, and (iv) spin frustration are required to realize the large negative MR. These latter requirements (iii) and (iv) are obvious since the MR was not observed in metallic Pd(Fe, Mn) and strong ferromagnetism would cause a spontaneous long-range cluster alignment into ferromagnetic domains, obviating the need for field alignment. For oxides, these requirements can be satisfied by forming a solid solution between a Stoner (such as $SrRuO_3$) or nearly Stoner (such as $CaRuO_3$ and Sr_2RuO_4) ferromagnet[37] and an antiferromagnetic insulator (such as $LaFeO_3$).[9]

Finally, we reiterate that the mechanisms of magnetism, conduction, and MR in these ruthernates are entirely distinct from those in manganates, for which mixed valence and Jahn-Teller distortion are essential. This is made obvious by noting some fundamentally different characteristics of the two systems. For example, the pressure dependence of T_C is positive for manganates because the increased bandwidth favors charge delocalization and double exchange,[38] but the opposite holds in $SrRuO_3$ because the increased bandwidth decreases $N(E_f)$, adding to the kinetic energy penalty for band polarization.[39] Nevertheless, the fundamental exchange mechanism of electron resonance between an occupied state and an empty state, at two neighboring cation sites, applies to both Ru^{4+}/Fe^{3+} in $Sr_{1-x}La_xRu_{1-x}Fe_xO_3$ and Mn^{3+}/Mn^{4+} in manganates. Therefore, a hybrid mechanism is entirely possible when both Ru and Mn coexist in the same system.[22]

ACKNOWLEDGMENTS

This work was supported by the National Science Foundation, Grant No. DMR 03-03458 and DMR00-79909. The authors gratefully thank R. Fisch for many stimulating discussions. They also want to thank W. Dmowski, T. Egami, S. Khalid, and W. Caliebe for help with the experiment at X19A, at the National Synchrotron Light Source, Brookhaven National Laboratory, which is supported by the U.S. Department of Energy, Division of Materials Sciences and Division of Chemical Sciences, under Contract No. DE-AC02-98CH10886.

*Author to whom correspondence should be addressed; Electronic address: iweichen@seas.upenn.edu

[1] A. P. Ramirez, J. Phys.: Condens. Matter **9**, 8171 (1997); M. Imada, A. Fujimori, and Y. Tokura, Rev. Mod. Phys. **70**, 1039 (1998); J. M. D. Coey, M. Viret, and S. von Molnar, Adv. Phys. **48**, 167 (1999); M. Salamon and M. Jaime, Rev. Mod. Phys. **73**, 583 (2001).

[2] P. D. Battle, T. C. Gibbs, C. W. Jones, and F. Studer, J. Solid State Chem. **78**, 2282 (1989); A. V. Powell, J. G. Gore, and P. D. Battle, J. Alloys Compd. **201**, 73 (1993); S. H. Kim and P. D. Battle, J. Magn. Magn. Mater. **123**, 273 (1993); S. H. Kim and P. D. Battle, J. Solid State Chem. **114**, 174 (1995); P. D. Battle, T. C. Gibb, A. J. Herold, S. H. Kim, and P. H. Munns, J. Mater. Chem. **5**, 865 (1995); E. J. Cussen, J. F. Vente, P. D. Battel, and T. C. Gibb, J. Mater. Chem. **7**, 459 (1997); P. D. Battle, G. R. Blake, T. C. Gibb, and J. F. Vente, J. Solid State Chem. **145**, 541 (1999); J. F. Vente and P. D. Battle, *ibid.* **146**, 163 (1999).

[3] Landolt-Bornstein, *Magnetic Properties of Non-Metallic Inorganic Compounds Based on Transition Elements* New Series, III/27 F1b (Springer-Verlag, Berlin, 1985).

[4] K.-I. Kobayashi, T. Kimura, H. Sawada, K. Terakura, and Y. Tokura, Nature (London) **395**, 677 (1998).

[5] Y. Tomioka, T. Okuda, Y. Okimoto, R. Kumai, K-I. Kobayashi, and Y. Tokura, Phys. Rev. B **61**, 422 (2000); H. Yanagihara, M. B. Salamon, Y. Lyanada-Geller, S. Xu, and Y. Moritomo, *ibid.* **64**, 214407 (2001); H. Q. Yin, J.-S. Zhou, J.-P. Zhou, R. Dass, J. T. McDevitt, and J. B. Goodenough, Appl. Phys. Lett. **75**, 2812 (1999).

[6] A. E. Berkowitx, J. R. Mitchell, M. J. Carey, A. P. Young, S. Zhang, F. E. Spada, F. T. Parker, A. Hutton, and G. Thomas, Phys. Rev. Lett. **68**, 3745 (1992); J. Q. Xiao, J. S. Jiang, and C. L. Chien, *ibid.* **68**, 3749 (1992); C. L. Chien, Annu. Rev. Mater. Sci. **25**, 129 (1995).

[7] T. He and R. J. Cava, Phys. Rev. B **63**, 172403 (2001).

[8] I. I. Mazin and D. J. Singh, Phys. Rev. B **56**, 2556 (1997).
[9] A. Mamchik and I.-W. Chen, Appl. Phys. Lett. **82**, 613 (2003).
[10] A. Mamchik, Ph.D. dissertation, University of Pennsylvania, 2003.
[11] H. Kobayashi, M. Nagata, R. Kanno, and Y. Kawamoto, Mater. Res. Bull. **29**, 1271 (1994).
[12] A. C. Larson and R. B. Von Dreele, Los Alamos National Laboratory Report LAUR 86–748, 2000.
[13] M. Marezio and P. D. Dernier, Mater. Res. Bull. **6**, 23 (1971).
[14] S. Ebbinghaus, Z. Hu, and A. Reller, J. Solid State Chem. **156**, 194 (2001); Z. Hu, H. von Lips, M. S. Golden, J. Fink, G. Kaindl, F. M. F. de Groot, S. Ebbinghaus, and A. Reller, *ibid.* **61**, 5262 (2000); R. S. Liu, L.-Y. Jang, H. H. Hung, and J. L. Tallon, *ibid.* **63**, 212507 (2001); G. V. M. William, L.-Y. Jang, and R. S. Liu, *ibid.* **65**, 064508 (2002).
[15] D. Kim, B. L. Zink, F. Hellman, S. McCall, G. Cao, and J. E. Crow, Phys. Rev. B **67**, 100406 (2003).
[16] D. Treves, J. Appl. Phys. **36**, 1033 (1965); W. C. Koehler and E. O. Wollan, J. Phys. Chem. Solids **2**, 100 (1957).
[17] K. Binder and A. P. Young, Rev. Mod. Phys. **58**, 801 (1986).
[18] T. Moriya, *Spin Fluctuations in Itinerant Electron Magnetism* (Springer-Verlag, Berlin, 1985).
[19] See, for example, A. L. Efros and M. Pollak, *Electron-Electron Interactions in Disordered Systems* (Elsevier Sci., New York, 1985), pp. 297, 303, 432.
[20] S. C. Gausepohl, M. Lee, K. Char, R. A. Rao, and C. B. Eom, Phys. Rev. B **52**, 3459 (1995); L. Klein, A. F. Marshall, J. W. Reiner, C. H. Ahn, T. H. Geballe, M. R. Beasley, and A. Kapitulnik, J. Magn. Magn. Mater. **188**, 319 (1998).
[21] For A-site substitution: G. Cao, S. McCall, M. Shepard, J. E. Crow, and R. P. Guertin, Phys. Rev. B **56**, 321 (1997); T. He, Q. Huang, and R. J. Cava, *ibid.* **63**, 024402 (2000); H. Nakatsugawa, E. Iguchi, and Y. Oohara, J. Phys.: Condens. Matter **14**, 415 (2002). For B-site substitution. Ref. 7; G. Cao, S. McCall, M. Shepard, and J. E. Crow, *ibid.* **56**, 321 (1997).
[22] L. Pi, A. Maignan, R. Retoux, and B. Raveau, J. Phys.: Condens. Matter **14**, 7391 (2002).
[23] P. B. Allen, H. Berger, O. Chauvet, L. Forro, T. Jarlborg, A. Junod, B. Revaz, and G. Santi, Phys. Rev. B **53**, 4393 (1996); L. Klein, J. S. Dodge, C. H. Ahn, G. J. Snyder, T. H. Geballe, M. R. Beasley, and A. Kapitulnik, Phys. Rev. Lett. **77**, 2774 (1996).
[24] For Fe: N. Hamada, H. Sawada, and K. Terakura, in *Spectroscopy of Mott Insulators and Correlated Metals*, edited by A. Fujimori and Y. Tokura (Springer-Verlag, Berlin, 1995) p. 95; T. Arima, Y. Tokura, and J. B. Torrance, Phys. Rev. B **48**, 17006 (1993). For Ru: J. S. Lee, Y. S. Lee, T. W. Noh, K. Char, J. Park, S.-J. Oh, J.-H. Park, C. B. Eom, T. Takeda, and R. Kanno, Phys. Rev. B **64**, 245107 (2001); Y. S. Lee, J. S. Lee, T. W. Noh, D. Y. Byun, K. S. Yoo, K. Yamaura, and E. Takayama-Muromachi, e-print cond-mat/0207012 V.1., 30, June 2002 (unpublished).
[25] Goodenough also predicted a moderately positive J_{FeRu}, but his argument is based on the interaction between an empty Ru^{4+} e_g and a half-full Fe^{3+} e_g. This argument would also predict a ferromagnetic coupling between Mo^{5+} and Fe^{3+}, which is not supported by the experiment. See J. B. Goodenough, *Magnetism and the Chemical Bond* (Interscience, NewYork, 1963), p. 174.
[26] J. Lindén, T. Yamamoto, M. Karppinen, H. Yamauchi, and T. Pietari, Appl. Phys. Lett. **76**, 2925 (2000); J. H. Jung, S.-J. Oh, M. W. Kim, T. W. Noh, J.-Y. Kim, J.-H. Park, H.-J. Lin, C. T. Chen, and Y. Moritomo, Phys. Rev. B **66**, 104415 (2002).
[27] P. W. Anderson, Phys. Rev. **124**, 41 (1961).
[28] A. M. Clogston, H. T. Matthias, M. Peter, H. J. Williams, E. Corenzwit, and R. C. Cherwook, Phys. Rev. **125**, 541 (1962).
[29] A. Oswald, R. Zeller, and P. H. Dederichs, Phys. Rev. Lett. **56**, 1419 (1986).
[30] P. A. Wolff, Phys. Rev. **124**, 1030 (1961).
[31] A. M. Clogston, Phys. Rev. **125**, 439 (1962)
[32] F. M. Mueller, A. J. Freeman, J. O. Dimmock, and A. M. Furdyna, Phys. Rev. B **1**, 4617 (1970).
[33] G. G. Low and T. M. Holden, Proc. Phys. Soc. London **89**, 119 (1966).
[34] W. M. Star, S. Foner, and E. J. McNiff, Phys. Rev. B **12**, 2690 (1975).
[35] B. H. Verbeek, G. J. Nieuwenhuys, H. Stocker, and J. A. Mydosh, Phys. Rev. Lett. **40**, 586 (1978).
[36] G. Cao, Y. Xin, C. S. Alexander, and J. E. Crow, Phys. Rev. B **63**, 184432 (2001).
[37] I. I. Mazin, D. A. Papaconstantopoulos, and D. J. Singh, Phys. Rev. B **61**, 5223 (2000); G. Cao, C. S. Alexander, S. McCall, J. E. Crow, and R. P. Guertin, Mater. Sci. Eng., B **63**, 76 (1999).
[38] Y. Moritomo, H. Kuwahara, Y. Tomioka, and Y. Tokura, Phys. Rev. B **55**, 7549 (1997).
[39] F. Le Marrec, A. Demuer, D. Jaccard, J. M. Triscone, M. K. Lee, and C. B. Eom, Appl. Phys. Lett. **80**, 2338 (2002); J. J. Neumeier, A. L. Cornelius, and S. Schilling, Physica B **198**, 324 (1994); M. Shikano, T.-K. Huang, Y. Inaguma, M. Itoh, and T. Nakamura, Solid State Commun. **90**, 115 (1994).
[40] J. Zaanen, G. A. Sawatzky, and J. W. Allen, Phys. Rev. Lett. **55**, 418 (1985).